Indian Journal of Chemical Technology
Vol. 27, January 2020, pp. 67-72

Corrosion investigation of nickel base superalloys in simulated high level waste medium using electrochemical impedance spectroscopy

Pradeep Kumar Samantaroy*[1,2] & Girija Suresh[1]

[1]Indira Gandhi Centre for Atomic Research, Kalpakkam 603 102, India
[2]Rayagada Autonomous College, Rayagada 765 001, India
E-mail: pksroy82@gmail.com

Received 12 March 2017 ; accepted 22 April 2019

Nickel base superalloys (Alloy 600, 690 and 693) under as-received and heat treated (solution-annealed and sensitized) condition have been assessed by electrochemical impedance spectroscopic technique for their corrosion behavior in 3 M HNO_3 and simulated high level waste medium at 25°C. All the alloys in all the conditions (as-received, solution-annealed and sensitized) show higher polarization resistance in 3 M HNO_3 compared to simulated high level waste. The solution-annealed specimens for Alloy 690 and Alloy 693 show near capacitive behaviour in a larger ranger of frequency. Among the three alloys, Alloy 690 show highest polarization resistance followed by Alloy 693 and Alloy 600, due to the better stability of passive oxide layer. In contrast, the decreased polarization resistance for Alloy 600 specimens imply deterioration or reduction in the passive film stability.

Keywords: Nickel alloys, Electrochemical impedance spectroscopy, Sim. HLW, Heat treatment

Electrochemical impedance spectroscopy (EIS) is a powerful and well established technique used for the characterization of electrochemical properties of the materials and their interfaces in different environments. Impedance is the opposition to the flow of current, which is given by the ratio of applied voltage to the resulting current. It is the combination of resistance and reactance in an electrochemical system[1]. The locus of impedance as a function of angular frequency is called impedance spectrum. This technique involves the determination of cell impedance, in response to a small AC signal at any constant DC potential (preferably at the OCP to minimize the DC currents), over frequencies ranging from a micro to mega-hertz.

Impedance spectroscopy is widely used to analyze the complex properties in a material such as dielectric properties, mass transport, defect density, passive film stability, coating degradation, microstructural and compositional effects on the conductance of solids, and impedance of biological membranes[2-7]. The major advantages of this technique are its nondestructive nature due to the application of very low potential, the rapidity in measurements with potentiostat and frequency response analyzers and data processing using appropriate software programs. Also, it has the advantage of providing the required information on the formation/interfacial reactions and protection mechanisms of a given surface layer[8,9]. On the other hand, the difficulty in interpreting the data is major deficiency of this technique. The most common approach is based on the equivalent circuit concept, exemplified in the model of Randles[10].

EIS technique has been successfully applied to the study of corrosion systems for a few decades and is proved to be a powerful and accurate method for measuring corrosion rates. In corrosion experiments, generally 10 to 50 mV sinusoidal voltage signal is applied to a corroding electrode interface and the current signal resulting at the same excitation frequency is measured. The impedance is measured over a domain of discrete frequencies ranging from 0.001 to 10^6 Hz. At the high-frequency end, the interfacial capacitance will dominate and hence, only the electrolyte's resistance will contribute to the impedance. At lower frequencies, interfacial resistance will contribute to the impedance. Electrochemical and diffusional processes associated with corrosion are detected at frequencies in the range 10-10^{-6} Hz. However, below the frequency of 10^{-3} Hz, the metallic electrochemical interface will become unstable and reliable measurements may not be possible[1].

Impedance Z, can be expressed in complex number notation as

$$Z = Z' + jZ'' \quad \ldots (1)$$

where Z' and Z" represent the real and Z" represents the imaginary components respectively. Nyquist plot and Bode plot are two types of diagrams which are most frequently used for the graphical representation of impedance data. In the Nyquist plot, the impedance is represented by a real part and an imaginary part. In the Bode plot, the modulus of the impedance and the phase angle are both plotted as a function of frequency. Nyquist plot allows an easy prediction of the properties of the electrode-electrolyte interface; however, it does not provide the information regarding the frequency dependence of impedance[11, 12]. Bode plot provides all the necessary information for clear interpretation of the results. The interpretation of the impedance data from either Nyquist or Bode plot is carried out by means of electrical equivalent circuit consisting of circuit elements like charge transfer resistance (Rp), Solution resistance (R_S) and Capacitance of double layer (CΩ). In order to account for non-ideal behaviour of capacitance, real capacitance is replaced by constant phase element (CPE) whose impedance is given by Eq 2.

$$Z_{CPE} = 1/[T(j\omega)^n] \quad \ldots(2)$$

where T and n are frequency-independent fit parameters, $j = (-1)^{1/2}$ and $\omega = 2\pi f$, where f is the frequency in Hz.

n is defined as $n = 1 - 2\alpha/180$, where α is the depression angle (in degree). When n = 1, CPE describes an ideal capacitor.

In our previous investigations, corrosion behavior of three nickel base superalloys (Alloy 600, Alloy 690 and Alloy 693) were studied for the nuclear high level waste (HLW) storage application in as-received as well as heat treated condition using electrochemical polarization technique in simulated HLW, compared against 3 M HNO_3[13-15]. In the present investigation, the corrosion behavior is accessed by electrochemical impedance spectroscopic technique in simulated HLW medium.

Experimental Section

Material and specimen preparation

The chemical composition of the testing materials (Alloy 600, 690 and 693) are given in Table 1.

The conditions of heat treatment to carry out solution annealing (SA) and sensitization (SEN) are tabulated in Table 2. The as-received specimens were solution-annealed according to the temperature and time listed in Table 2 and were immediately quenched in water. Solution annealing was carried out to dissolve the pre-existing carbides and other precipitates in the matrix. Few of the solution-annealed specimens were further heat treated at the sensitization condition as per Table 2 and were allowed to cool in air to induce sensitization.

The as-received condition and heat treated (solution-annealed and sensitized) specimens in the dimension of 10mm × 10 mm (exposure area approximately 1 cm^2), were polished with 600 grit silicon carbide paper, mounted with resin and then further polished up to diamond finish. The specimens were cleaned with soap solution and further cleaned with acetone. These specimens were used for the electrochemial experiments.

Test solution

The experiments were carried out in two different environments, 3 M HNO_3 and simulated HLW at 25°C. Oxide or nitrate of corresponding elements mentioned in the Table 3 were taken in the required stoichiometric ratio and were dissolved in 3 M HNO_3. The composition of such simulated HLW solution prepared was used for the electrochemical experiments.

Electrochemical measurement

The instrumentation for carrying out the impedance measurement consisted of a potentiostat and an electrochemical cell. The electrochemical cell for conducting the study consisted of (a) working electrode i.e. specimen to be tested, (b) a non-polarizable counter electrode for completing the circuit, and (c) a reference electrode with respect to which potential has to be applied. Reference electrode was separated from the solution by luggin probe, and was placed close to the working electrode to eliminate the effect of solution resistance. In the present investigation the nickel base specimens were used as working electrode, platinum as counter electrode and saturated calomel electrode (SCE) as reference

Table 1 — Chemical composition of Ni base superalloys

Element	Ni	Cr	Fe	C	S	Mn	Cu	Si	Ti	Nb	N	Al	Mo
Alloy 600	74.2	14.7	9.6	0.03	0.008	0.53	0.30	0.15	0.26	-	-	0.3	0.30
Alloy 690	60	29.6	9.05	0.017	0.0013	0.21	<0.01	0.25	0.2	0.02	68 ppm	-	-
Alloy 693	60.9	29.3	3.96	0.097	0.002	0.19	<0.02	0.04	0.42	1.86	-	3.19	-

electrode. Experiments were carried out at the solution temperature of 25°C in 3 M HNO_3 and simulated HLW. The specimens were allowed to equilibrate for 30 min and the open circuit potential (OCP) was monitored. The impedance data were recorded using an AUTOLAB PGSTAT30 FRA system, at the OCP and frequency range was adjusted from 100 KHz to 0.01 Hz with an applied AC perturbation of 10 mV. The impedance data were analyzed by a commercial software package "NOVA". According to literature, values of error less than 5% in modeling of EIS results give the best electrochemical interpretation. Constant phase element has been used in the present investigation to obtain better fit for the experimental data, which would represent the capacitance of the passive oxide layer. The impedance expression of CPE is expressed in Eq 2.

Table 2 — Heat treatment parameters

Material		Temp (°C)	Time (min)
Alloy 600	SA	1120	60
	SEN	800	60
Alloy 690	SA	1150	30
	SEN	700	60
Alloy 693	SA	1050	30
	SEN	700	60

Table 3 — Composition of the simulated HLW solution.

Element	Conc. (gL^{-1})	Valance state	Reagent used
Fe	0.72	+3	$Fe(NO_3)_3$
Cr	0.119	+6	CrO_3
Ni	0.107	+2	$Ni(NO_3)_2.6H_2O$
Na	5.5	+1	$NaNO_3$
K	0.224	+1	KNO_3
Cs	0.315	+1	$Cs\ NO_3$
Sr	0.031	+2	$Sr(NO_3)_2$
Zr	0.004	+4	$ZrO(NO_3)_2$
Ba	0.064	+2	$Ba(NO_3)_2$
La	0.18	+3	La_2O_3
Ce	0.06	+3	$Ce(NO_3)_3.6H_2O$
Pr	0.09	+3, +4	Pr_6O_{11}
Nd	0.12	+3	Nd_2O_3
Sm	0.0855	+3	Sm_2O_3
Y	0.06	+3	Y_2O_3
U	6.34	+4, +6	U_3O_8

Results and Discussion

The electrochemical impedance spectroscopic results of the nickel base superalloys under as-received condition, obtained at the OCP in 3 M HNO_3 and simulated HLW medium, are represented in Fig. 1 in the form of Nyquist plots, in which the imaginary impedance (Z'') is plotted against the real time impedance (Z'). It could be noticed from the plots that the impedance features were similar for all the three alloys in both the media, i.e. one depressed semicircle over the whole frequency range and all of them are characteristic of capacitive behavior. The formation of such a semicircle arc is attributed to the charge transfer process at the electrode/electrolyte interface and it relates the changes in the passive oxide property to the chemical composition[16-18]. This indicates that there is one interfacial reaction process over the measured frequency range. However, a distinct difference was observed in all the impedance spectra in 3 M HNO_3 and in simulated HLW. The semicircle radius was smaller in simulated HLW compared to that in 3 M HNO_3 for all the three alloys. The larger semicircle radius in 3 M HNO_3 indicated a better passive film stability and hence, better corrosion resistance.

Figure 2 shows the bode plots of as-received nickel base alloys in 3 M HNO_3 and in simulated HLW. All the specimens in both the media showed only one time constant. The EIS spectra for all the three alloys

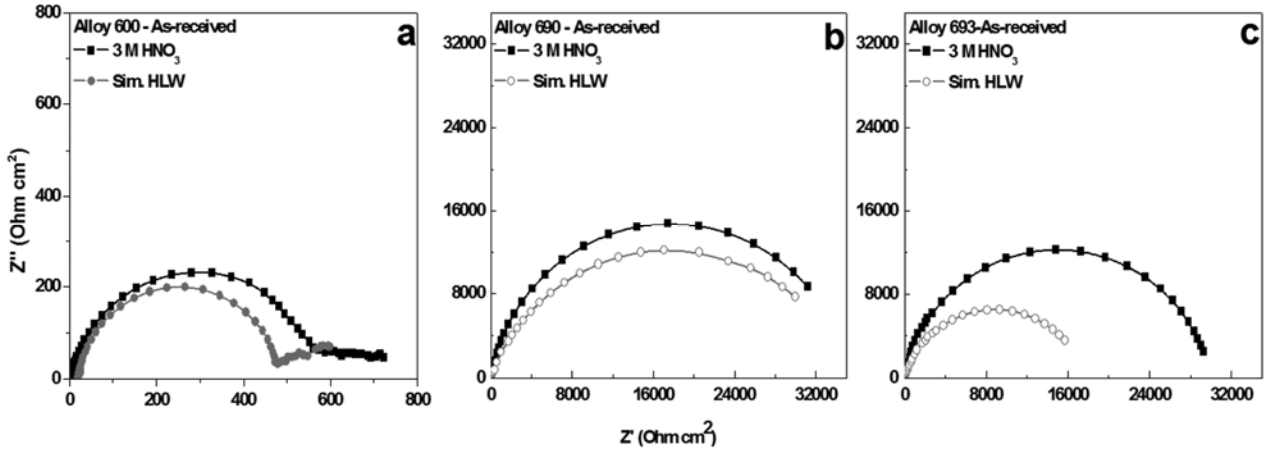

Fig. 1 — Nyquist plot for as-received (a) Alloy 600 (b) Alloy 690 (c) Alloy 693

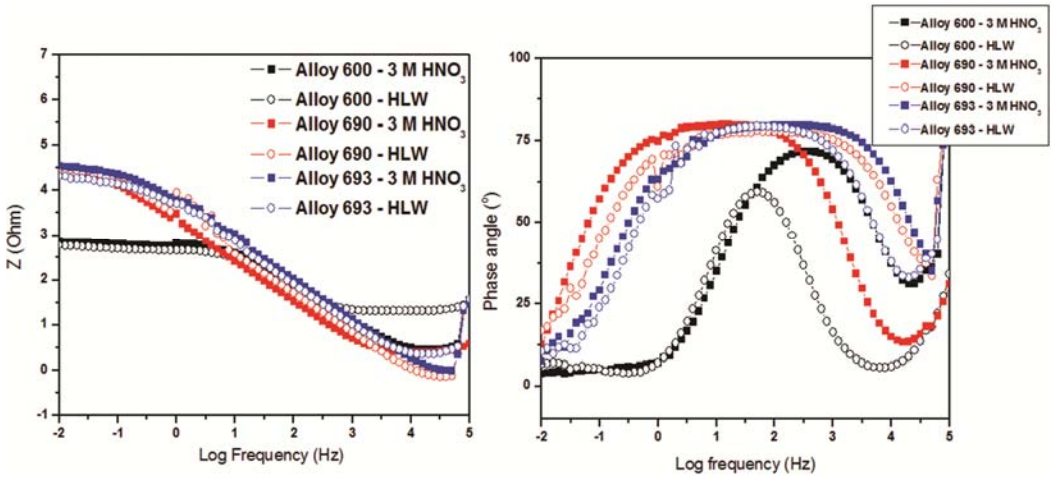

Fig. 2 — Bode plot of as-received specimens in 3 M HNO_3 and Sim. HLW

showed resistive property in the low and high frequency region and near capacitive property in the mid frequency region. Alloy 690 and 693 showed capacitive property in between the frequency region of 10^0 to 10^3 however, Alloy 600 showed larger resistive property and a narrow capacitive region of 10^1 to 10^2 Hz with a very small phase angle. The difference in magnitude of Z between Alloy 690 and Alloy 693 is almost negligible whereas the difference compared to Alloy 600 is more than of one order (Fig. 3a). The low impedance values of Alloy 600 compared to Alloy 690 and 693 shows a comparatively thin and less stable oxide film over the surface.

The experimental data from Fig. 1 and Fig. 2 are fitted in to the Randles circuit (given in Fig. 3) and the electrochemical parameters derived from the fitting are listed in Table 4. The circuit has the element arrangement of R_S (CPE$\|R_P$), where R_S is the solution resistance which depends on the resistivity of the solution, the electrode and cell geometry[19] , R_P is the polarization resistance which represents the resistance of the passive film as a result of its ionic conductivity and CPE is the constant phase element which corresponding to the capacitance parameter of the passive film due to its dielectric properties[20]. Replacing the capacitor by CPE is a common practice in the empirical EIS models.

It could be observed from Table 4 that all the alloys showed higher R_P value in 3 M HNO_3 compared to simulated HLW. The decrease in R_P could be attributed to the increased ionic conductivity through the passive film or thinning of passive film, resulting in the non-protective property[21]. The R_P is the sum of the film resistance and the charge transfer resistance. The charge transfer processes take place at the metal/film or

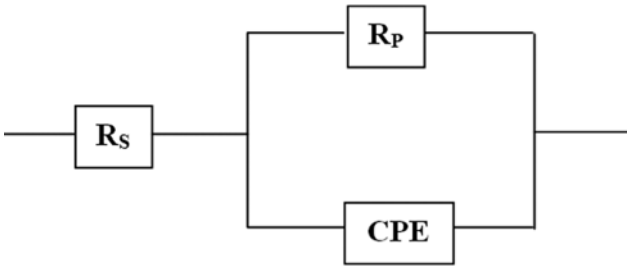

Fig. 3 — Equivalent circuit used for EIS analysis

Table 4 — Electrochemical parameters derived from EIS curves (as-received specimens)

Material	Medium	R_s (Ω cm^2)	R_p (kΩ cm^2)	CPE (Fcm^{-2} S^n)	n
Alloy 600	3M HNO_3	2.17	0.124	33.1x10^{-6}	0.908
	Sim. HLW	1.90	0.100	37.5 x10^{-6}	0.885
Alloy 690	3M HNO_3	2.02	35.4	42.2 x10^{-6}	0.885
	Sim. HLW	0.45	35.4	57.9 x10^{-6}	0.786
Alloy 693	3M HNO_3	0.75	30.0	34.0 x10^{-6}	0.873
	Sim. HLW	1.30	18.5	52.1 x10^{-6}	0.911

metal/electrolyte interface and control the rate of passive film growth on the specimens. The R_P values are strongly dependent on the passive film characteristics and are a measure of corrosion resistance. Higher R_P value implies good corrosion resistance (e.g. slow rate of metal ion release and oxide growth). Low capacitance value of the passive film indicates long term stability of the passive film[22-24] . Among the three alloys, highest R_P value was shown by Alloy 690 followed by Alloy 693 and Alloy 600. Higher R_P value observed in Alloy 690 could be attributed to increased stability of the passive oxide layer due to the formation of enriched oxide of chromium or nickel or both. In contrast, the decreased R_P values for Alloy 693 and Alloy 600 specimens imply

deterioration or reduction in the passive film stability. This is well in agreement with the results obtained XPS in our previous investigation[13,14] , which showed a stable passive film for Alloy 690 than Alloy 693 followed by Alloy 600, when passivated under simulated HLW. The The variation in R_S could be attributed to a small difference between the specimen and reference electrode in the EIS measurement. The values of the CPE parameter are relatively lower in 3 M HNO_3 compared to simulated HLW for the alloys (Table 4). The CPE parameter is used to represent double layer capacitance of the film/electrolyte interface. Lower value of CPE indicated that the ion adsorption occurring at the surface of the specimens in 3 M HNO_3 is low, thereby confirming the better corrosion resistance. Lower value of CPE also indicates the formation of thicker and more protective passive film on the surface whereas higher value indicates the non-homogeneous nature of film, which could be the result of local defects weakening the passive film.

The value of n (Table 4), which gives the deviation of capacitance of the passive film from the ideal capacitive behaviour was in the range 0.75-0.95. These values indicate that the deviation from purely capacitive behaviour was relatively small for all the alloys in both the media.

The electrochemical impedance spectroscopic results of the heat treated nickel base superalloys obtained at OCP in 3 M HNO_3 and simulated HLW medium, in the form of Nyquist plots are represented in Fig. 4 and Bode plots are represented in Fig. 5. Similar to the as-received specimens, in the heat treated condition also, one depressed semicircle was observed over the whole frequency range which indicates the characteristics of capacitive behaviour and one interfacial reaction process over the whole frequency range. The

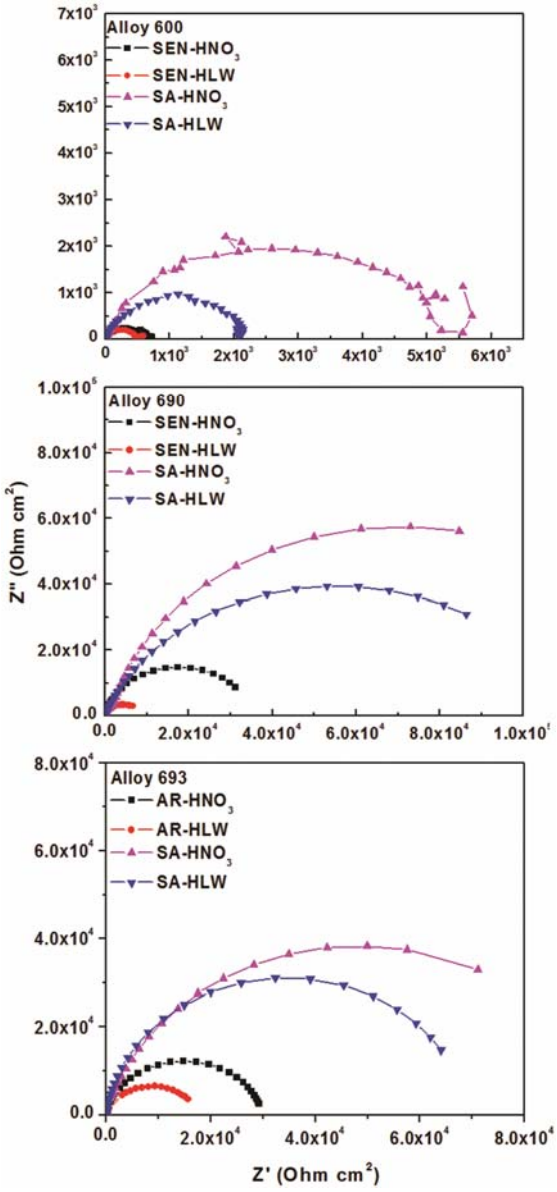

Fig. 4 — Nyquist plots of heat treated (a) Alloy 600 (b) Alloy 690 (c) Alloy 693

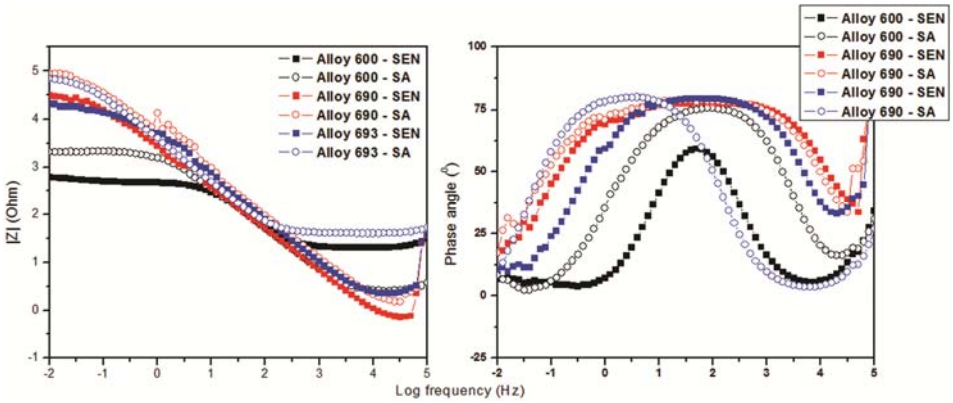

Fig. 5 — Bode plot of heat treated specimens in sim. HLW

Table 5 — Electrochemical parameter derived from EIS curves (heat treated specimens)

Material		Medium	R_s (Ω cm^2)	R_p (kΩ cm^2)	CPE F cm^{-2}S^n	n
Alloy 600	[a]SEN	3 M HNO_3	2.0	0.115	35.1×10^{-6}	0.887
		Sim. HLW	1.9	0.101	39.5×10^{-6}	0.885
	[b]SA	3 M HNO_3	2.0	5.55	55.6×10^{-6}	0.757
		Sim. HLW	2.0	2.14	73.7×10^{-6}	0.876
Alloy 690	SEN	3 M HNO_3	2.02	35.4	97.9×10^{-6}	0.885
		Sim. HLW	0.45	35.4	72.2×10^{-6}	0.786
	SA	3 M HNO_3	1.30	22.3	54.5×10^{-6}	0.947
		Sim. HLW	1.00	90	35.2×10^{-6}	0.871
Alloy 693	SEN	3 M HNO_3	0.75	30.0	34.0×10^{-6}	0.873
		Sim. HLW	1.30	23.5	54.5×10^{-6}	0.911
	SA	3 M HNO_3	0.65	69.1	45.6×10^{-6}	0.881
		Sim. HLW	1.0	90	60.3×10^{-6}	0.933

[a]Sensitized; [b]Solution-annealed

semicircle radius was smaller in the sensitized specimens as compared to the solution-annealed specimens. Similarly, the radius of semicircle in the simulated HLW was smaller than that in 3 M HNO_3 for all the three alloys. The larger semicircle radius indicated a better passive film stability and hence better corrosion resistance. These data were fitted to the Randles circuit (Fig. 3) and the electrochemical parameters obtained from fitting are reported in Table 5.

It could be observed from Table 5 that all the alloys showed higher R_P value for the solution-annealed specimens compared to the as-received and sensitized specimens. The values of the CPE parameter are relatively lower in solution-annealed specimens than the sensitized specimens for all the alloys; indicates less ion adsorption on the surface of solution annealed specimens. The superior behavior of solution annealed specimens compared as-received and sensitized specimens could be attributed to the homogeneous microstructures due to the dissolution of all precipitates after solution annealling, which was reported by us elsewhere[13,15] .

Conclusion

From the present study it can concluded that the solution-annealed specimens showed better corrosion resistance than the as-received specimens followed by the sensitized specimens. Similarly, all the specimens in all the conditions showed better resistance in 3 M HNO_3 than in sim. HLW. Among the three alloys, Alloy 690 showed highest polarization resistance followed by Alloy 693 and Alloy 600, due to the better stability of passive oxide layer. In contrast, the decreased polarization resistance for Alloy 600 specimens imply deterioration or reduction in the passive film stability.

References

1 Kelly R G, Scully J R, Shoesmith D W & Buchheit R G, *Electrochemical Techniques in Corrosion Science and Engineering*, (Marcel Dekker, Inc. New York), 2003.
2 Dygas J R, *Solid State Ionics*, 176 (2005) 2065
3 Betova I, Bojinov M, Karastoyanov V, Kinnunen P & Saario T, *Electrochim Acta*, 55 (2010) 6163.
4 Cabrera-Sierra R, Hallen J M, Vazquez-Arenas J, Vazquez G & Gonzalez I, *J Electroanal Chem*, 638 (2010) 51.
5 Ohtsuka T & Otsuki T, *Corros Sci*, 40 (1998) 951.
6 Kendig M & Mansfeld F & Tsai S, *Corros Sci*, 23 (1983) 317.
7 Freger V & Bason S, *J Membrane Sci*, 302 (2007) 1.
8 Zeller R L & Savinell R F, *Corros Sci*, 26 (1986) 389.
9 Popova A & Christov M, *Corros Sci*, 48 (2006) 3208.
10 Randles J E B, *Discuss Faraday Soc*, 1 (1947) 11.
11 Orazem M K & Tribollet B, in *Electrochemical impedance spectroscopy,* edited by M E Orazem & B Tribollet, (Wiley Inter-Science), 2008.
12 Macdonald J R & Johnson W B, in *Fundamentals of impedance spectroscopy*, edited by E Barsoukov & J R Macdonald, (John Wiley and Sons) 2005.
13 Samantaroy P K, Girija S, Krishna N G & Kamachi Mudali U, *J Mater Eng Perform*, 22 (2012) 1041.
14 Samantaroy P K, Girija S, Paul R, Kamachi Mudali U & Baldev Raj, *J Nucl Mater*, 27 (2011) 418.
15 Samantaroy P K, Girija S & Kamachi Mudali U, *Corrosion*, 68 (2012) 046001.
16 Hermas A A & Morad M S, *Corros Sci*, 50 (2008) 2710.
17 Ningshen S, Kamachi Mudali U, Amarendra G & Baldev Raj, *Corros Sci*, 51 (2009) 322.
18 Ningshen S, Kamachi Mudali U, Mukherjee P, Sarkar A, Barat P, Padhy N & Baldev Raj, *Corros Sci*, 50 (2008) 2124.
19 Sluyters-Rehbach M, *Pure Appl Chem*, 66 (1994) 1831.
20 Shukla A K, Balasubramaniam R & Bhargava S, *Intermetallics*, 13 (2005) 631.
21 Castro E B & Vilche J R, *Electrochim Acta*, 38 (1993) 1567.
22 Kamachi Mudali U, Kaul R, Ningshen S, Ganesh P, Nath A K, Khatak H S & Baldev Raj, *Mater Sci Tech*, 22 (2006) 1185.
23 Bojinov M, Betova I, Fabricius G, Laitinen T, Raicheff R & Saario T, *Corros Sci*, 41 (1999) 1557.
24 Sun M, Xiao K, Dong C & Li X, *Acta Metall Sin (Engl Lett)*, 23 (2010) 301.